Adsorption, Stretching and Breaking Processes in Single-Molecule Conductance of para-Benzenedimethanethiol in Gold Nanogaps: A DFT-NEGF Theoretical Study

Guan, Si-Yuan; Cai, Zhuan-Yun; Liu, Jia; Pang, Ran; Wu, De-Yin; Ulstrup, Jens; Tian, Zhong-Qun

Published in:
ChemElectroChem

Link to article, DOI:
10.1002/celc.202100184

Publication date:
2021

Document Version
Peer reviewed version

ChemElectroChem

Chemistry Europe
European Chemical Societies Publishing

Accepted Article

Title: Adsorption, Stretching and Breaking Processes in Single-Molecule Conductance of para-Benzenedimethanethiol in Gold Nanogaps: A DFT-NEGF Theoretical Study

Authors: Si-Yuan Guan, Zhuan-Yun Cai, Jia Liu, Ran Pang, De-Yin Wu, Jens Ulstrup, and Zhong-Qun Tian

To be cited as: *ChemElectroChem* 10.1002/celc.202100184

Link to VoR: https://doi.org/10.1002/celc.202100184

WILEY-VCH

10.1002/celc.202100184

Adsorption, Stretching and Breaking Processes in Single-Molecule Conductance of para-Benzenedimethanethiol in Gold Nanogaps: A DFT-NEGF Theoretical Study

Mr. Si-Yuan Guan, [△†] Mr. Zhuan-Yun Cai, [△†] Dr. Jia Liu,[†] Dr. Ran Pang, [†] Prof. De-Yin Wu,[†] Prof. Jens Ulstrup[‡], and Prof. Zhong-Qun Tian[†]*

[†]State Key Laboratory of Physical Chemistry of Solid Surface, Collaborative Innovation Center of Chemistry for Energy Materials, and Department of Chemistry, College of Chemistry and Chemical Engineering, Xiamen University, Xiamen, 361005, P. R. China

‡Department of Chemistry, Technical University of Denmark, DK-2800 Kongens Lyngby, Denmark

***Corresponding author**:

Prof. De-Yin Wu, email: dywu@xmu.edu.cn

[△]**First Co-authors:** Mr. Si-Yuan Guan and Mr. Zhuan-Yun Cai

Abstract

Electrical and mechanical properties of gold-*para*-benzenedimethanethiol (BDMT)-gold molecular junctions with different binding configurations have been investigated using density functional theory (DFT) combined with a non-equilibrium Green's function (NEGF) approach. We first determined the most stable structure in total electronic energy by geometry optimization of the molecular junction. We then studied how different stretching processes affect the conductance and the stretching forces. Particularly two stretching modes can bring about different conductance behavior. When only a single-end molecular contact in interfacial configurations at the top and bridge sites is stretched, the molecular conductance first decreases exponentially. This is followed by a flat platform, and finally produced an abrupt conductance drop from the fracture of interfacial chemical bond Au-Au. In the junction with a double-end stretching mode, the fracture of Au-S bond occurs either between the sulfur-bonded gold atom and the underlying Au surfaces, or at either of the two Au-S bonds in the double-end stretching mode at the top-pyramidal site. The latter interfacial structure consists of a four-Au-atom pyramidal structure adsorbed on gold surface, resulting in a sharp conductance increase just before complete fracture. This is closely associated with resonance tunneling of beta spin electrons in the critical fracture state of interfacial Au-S bonds in gold-BDMT-gold molecular junction.

Introduction

Developing trends in the field of molecular electronic devices and higher integration into smaller size[1,2] are represented by a broad variety of organic and inorganic molecules, and have been studied experimentally and theoretically over the past several decades.[3-5] Many novel phenomena of molecular electronics such as diode amplification, rectification, switching, quantum interference, ion sensing, and light-sensitive effects have been observed,[6-11] offering promising molecular electronic perspectives. To understand the electric properties of a single-molecule junction, which is the minimum functional unit, different techniques with high spatial resolution and fast response have been introduced[12-14] Widely used core experimental tools are scanning tunneling microscopy (STM), atomic force microscopy (AFM), and mechanically controllable break junctions (MCBJ).[15-19] In STM, the molecule is adsorbed between two metal electrodes, forming a metal tip-molecule-substrate metal junction. The retraction and extraction of the tip in metal electrodes lead to formation and fracture of the metal-molecule bond, respectively. Parallel recording of current-voltage curves and of the molecular conductance offers accompanying informative insight[20] Similar methodology is used in AFM and MCBJ tools, where the former is controlled by mechanical forces, while the latter is focused on the conductance of the molecular gaps.

The conductance of organic molecules sandwiched between two metal electrodes is, however, a subtle dynamic process, mapping of which requires information about several molecular conformations. These challenges might be a major reason why large disagreement between theoretically and experimentally determined conductance values even for simple molecules and even among seemingly similar experiments remains. AFM was recently used to record simultaneously the conductance and the force applied to molecular wires during the mechanical stretching of molecular junctions.[16] Such data provide new insight into the nature of the molecule-electrode bonding and intermolecular interactions.[21-24] However, the binding structural evolution at the atomic level during the stretching processes of a metal-molecule-metal junction is still a key experimental and theoretical challenge.

Density functional theory (DFT) calculations have been used to address the interfacial structures and electric properties in nanoscale junctions. This theoretical approach, however, overestimates the molecular conductance of conjugated molecules by one or two orders of magnitude. This is due to the underestimation of the HOMO/LUMO bandgap of the molecules in dynamic structure changes. But combined with the non-equilibrium Green's function (NEGF) approach, DFT is still meaningful as a basis for the relationship between conductance and interfacial structures in molecular junctions.[25] In addition, DFT is important for understanding the correlation between the electrical and mechanical properties of molecular junctions in the dynamic evolution processes,[26] enabling determining the stretching force required to break the molecular junctions and the identity of the chemical bonds broken. For example, the dynamic evolution of thiyl molecules sandwiched between two metal electrodes under pulling forces is studied extensively both experimentally and theoretically.[27,28] There are two main fracture positions in the S-Au or Au-Au bonds. Different initial bonding configurations affect significantly this fracture process. In a recent study, good agreement between theory and experiments was obtained for simple alkanedithiol molecules but the conductance particularly for molecules with aromatic groups, such as oligo(phenylene ethynylene) (OPE), calculated values theoretically are often larger than experimental values by up to two orders of magnitude.[29] As noted, the main reason for this discrepancy is overestimation of the energy of the highest occupied molecular orbital (HOMO), which is close to the Fermi levels of both gold electrodes.

In this paper, we present a theoretical study of electrical and mechanical properties for gold-benzenedimethanethiol (BDMT)-gold molecular junction to probe the critical information on its structure and conductance evolution under stretching process. BDMT is chosen as the probe molecule, because its single-molecular junction properties have been characterized in lots of researches experimentally[30-33] and theoretically in details.[11,29,33-37] We first design different initial bonding configurations to explore the total energy-distance curves, the structural evolution and fracture forces in the pulling processes of molecular junctions. We then calculate the conductance of Au-BDMT-Au molecular junctions with different binding structures during stretching process. It is

worth noting that the change of molecular conductance during the stretching process is quite sensitive to the interfacial structures. Finally, we compute the electronic transmission spectra and the molecular projected self-consistent Hamiltonian (MPSH) of single-molecule junctions at different stretching distances. The conclusion that conductance of molecular junctions is dependent on the interface energy level alignment and overall electron density distribution of molecules are reached. Such a detailed analysis that the relation of interfacial configurations and conductance of molecular junctions by changing different adsorption structures and stretching methods is very important to understand the electronic transport properties of molecular junctions. It can be expected to become a useful guide to control mechanically over molecular conductance.

Theoretical and Computational Details

Our molecular junction model is based on the Au-BDMT-Au junction model(Figure 1, upper panel). The electrode structure is based on a semi-infinite periodical approach for the left and right leads, i.e. three layers (3×3) of Au atoms with a face-centered-cubic crystal structure of the (111) surface. The central region consists of a 5-layer Au (3×3)-molecule-5-layer Au (3×3). We designed three adsorption configurations of the BDMT molecular junctions, i.e. top-pyramidal, top, and hollow sites (Figure 1a, b and c, respectively). We used these as a basis to study the relationship between electronic and mechanical properties.

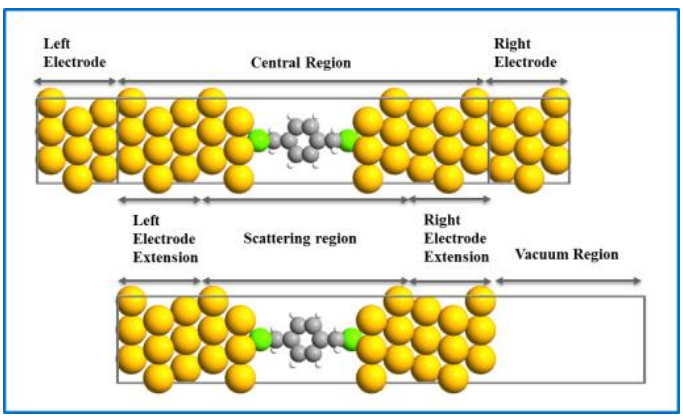

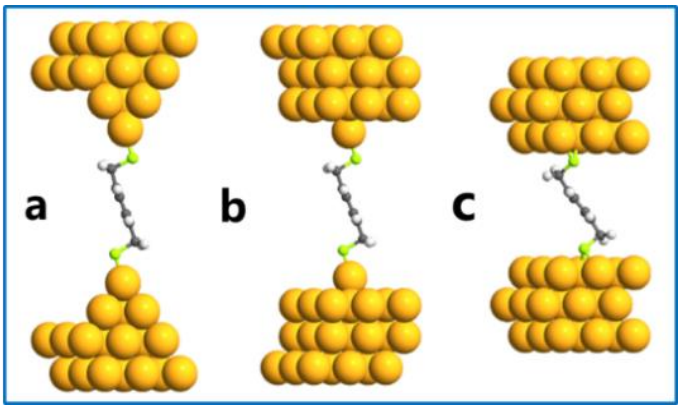

Figure 1. (Upper) The structures of the molecular junction with left electrode, central region, and right electrode and the only central region structure with a vacuum spacing region in the bottom. (Lower) Au-BDMT-Au molecular junction with different adsorption models. (a) Top-pyramidal site; (b) Top site; (c) Hollow site.

We firstly carried out structure optimization of the different molecular junction length under stretching process, using the GGA-PBE exchange-correlation (XC) functional approach.[38] The double-ζ polarized (DZP) basis set was used for carbon, hydrogen, and sulfur atoms, while a single-ζ polarized (SZP) basis set was employed for the gold atoms. The mesh cutoff energy of 75 Hartree was used. The 5 × 5 × 1 k grid sampling was used in the geometry optimization, and the 10 × 10 × 100 k point sampling with the Monkhorst-Pack scheme did in the quantum transport calculations in order to improve the accuracy. The geometry optimization and structural relaxation of the central region were performed with sufficient vacuum spacing (minimum of 12 Å) to prevent interaction between the periodic images. A relaxation procedure was carried out to ensure that the Hellmann-Feynman force acting on the atoms is less than 0.05 eV/Å.[39,40] All the calculations in the present work were performed using the Atomistix Toolkit package (ATK).[41]

To understand the relationship between the nanogap structure and single-molecule conductance during the stretching process, we used two models to simulate the structure evolution of the molecular junction. In the first model, the molecular junction was stretched by double-end stretching along the Z axis direction. In the second model, only a single end was stretched as shown in Figure 2.

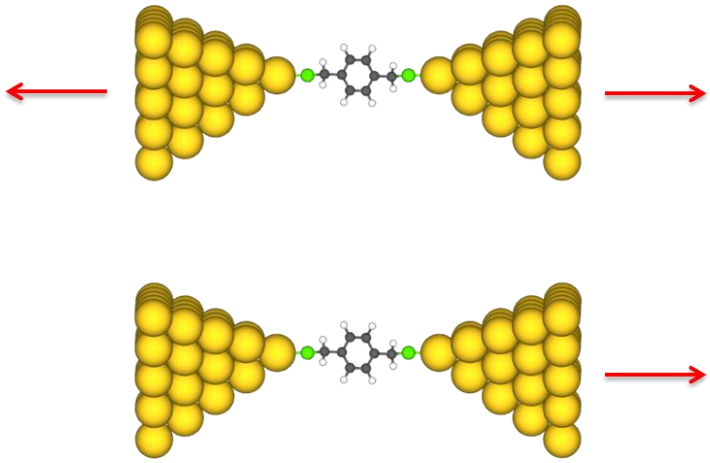

Figure 2. Schematic of a molecular junction stretched in double-end (top) and single-end model (bottom). Red arrows represent the stretching direction.

The initial vertical distances between single-crystal surface of left and right electrodes and the S atom were set as 1.71, 2.34, and 2.30 Å at bridge, top, and top-pyramidal sites, respectively. We first contracted the molecular junctions by the Au-S bond distance until about 2.30 – 2.40 Å, corresponding to the sulfur atom binding at the top site.[37,42-45] Following contraction, we pulled them apart gradually, until the bond fission occurred. In the stretching process, we obtained a series of optimized structures at given distances, as shown in SI, and built the relationship between the distance and total electronic energy, stretching force, and molecular conductance.

According to the Landauer-Büttiker formula,[46] the tunneling current and the electrical conductance g through a molecular junction at zero bias voltage and finite temperature, are written as

$$I = \frac{2e}{h}\int_{-\infty}^{+\infty} T(E)[f(E,\mu_1) - f(E,\mu_2)]\mathrm{d}E \qquad (1)$$

$$g = \frac{\mathrm{d}I}{\mathrm{d}V} \qquad (2)$$

where μ_1 and μ_2 are the electrochemical potentials of the electrons in the left and right electrodes, respectively, $f(E,T) = [e^{(E-E_F)/k_BT} + 1]^{-1}$ is the Fermi-Dirac distribution function, k_B is Boltzmann's constant, and e the electronic charge. $T(E)$ is the transmission coefficient, representing the probability of electrons transferring from the

source to the drain electrode. When the gold-BDMT-gold junction locates at zero bias voltage, the electrochemical potentials of both electrodes are the same ($\mu = \mu_1 = \mu_2$). The conductance of molecular junctions is mainly contributed by transmission coefficient of the Fermi level E_F of gold electrodes. With a bias V applied between the electrodes, the electrochemical potentials of source and drain electrodes become $\mu + V/2$ and $\mu - V/2$, respectively. In the case, the integral of transmission function $T(E)$ at an energy E over a bias window of V contribute to net current. The transmission coefficient is calculated using the NEGF approach[47,48]

$$T(E) = Tr[G(E)\Gamma_1 G^{\dagger}(E)\Gamma_2] \quad (3)$$

where Γ_1 and Γ_2 are broadening functions, which include the imaginary parts of the self-energy caused by the interaction of the molecular wire with the two electrodes, describing the coupling strength between the electrodes and the molecular wires. $G(E)$ and $G^{\dagger}(E)$ are Green's functions determined by the Hamiltonian of the molecular device. In our calculations, a larger k-points set of 10 × 10 was used in the calculation of the transmission spectra in order to improve the accuracy of the *T-E* and *I-V* curves. Such settings lead to well converging transmission curves.[49,50]

Results and Discussion

Relative Stability and Stretching Forces. We consider three initial contact geometries to probe simultaneously the mechanical and electrical properties in the stretching process, as depicted in Figure 1. Molecules were attached to the top-pyramidal, top and bridge sites, respectively. Figure 3 shows variation of total energies and stretching forces with stretching lengths of optimized Au-BDMT-Au molecular junctions by two stretching modes for the BDMT molecule binding to the top-pyramidal site. In order to make clearer, we firstly define the relative stability according to the total electronic energy. As shown in Figure 3a, the total electronic energy of the junction displays a minimum, which was referred to as the zero point of the equilibrium geometry of the molecular junction. The molecular junction length of the zero point is 3.27 nm and the relative energy is referred as that at this point. When the system length is stretched from

the minimum, the total electronic energy increases. The energy variation is very similar to a harmonic potential energy curve, indicating an elastic structure evolution of the system under stretching. This is followed by an abrupt decrease in the total electronic energy for the single-end and double-end stretching model when the molecular junction lengths are stretched to 3.20 Å nm and 3.80 Å, respectively, with respect to the energy equilibrium point, indicating the bond fission between the electrode and the molecule. And both fractures occur at the Au-S bond. The fracture distance is slightly longer for the double-end stretching model than for the single-end stretching model. This is also reflected in the stretching force curves of the gold-BDMT-gold junctions (Figure 3b). We defined the force applied to the junction in the stretching process as $F_Z = \frac{\partial E_{\text{tot}}}{\partial Z}$, where E_{tot} is the total energy of the junction at each step and Z represents the elongation of the system. This can be understood from the tension shared uniformly for double-end stretching. In the double-end stretching model, bond fracture happens at both ends, while only a single end is involved in the single-end stretching model.

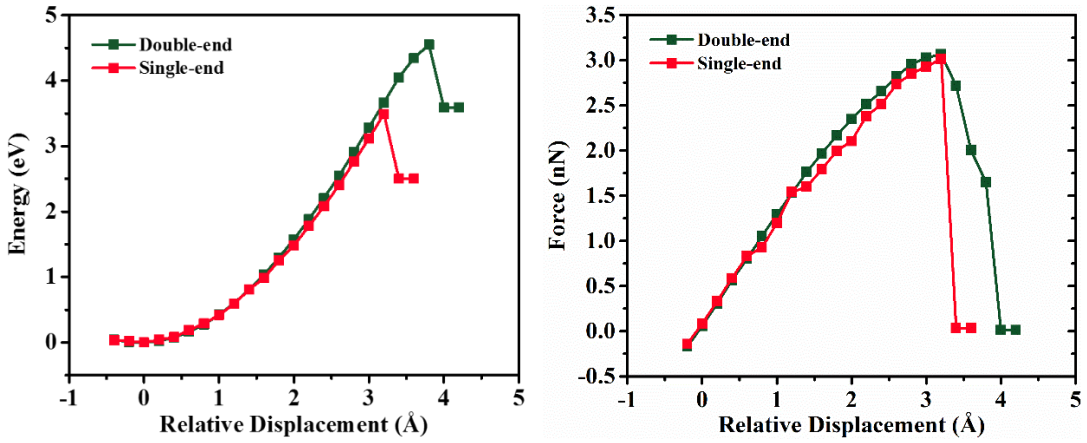

(a) (b)

Figure 3. Total electronic energies (a) and stretching forces (b) of the optimized Au-BDMT-Au molecular junctions of single (red) and double-end (black) bound BDMT with different lengths (relative to the lowest energy in each series).

Figure 3b shows the relationship between the stretching force and the length of molecular junctions. When the junctions are stretched to a certain length with the relative displacement of 3.20 Å, both stretching forces reach a similar maximum that are 19.13 and 19.34 eV/nm (3.07 nN and 3.10 nN) for single and double-end stretching

modes, respectively. For the single-end stretching mode, the fracture happens, when the stretching force reaches maximum. However, the molecular junction breaks down with the relative displacement of 3.80 Å in the double-end stretching mode, and the fracture force is 1.65 nN. The double-end stretching junction has a slightly longer fracture process than the single-end stretching one due to the tension force shared more uniformly in double-end stretching system. The fracture force of double-end stretching mode is more near to 1.97 nN from experimental data.[52,53] This is closely associated with the experimental conditions of the force loading rate when theoretical values are compared with experimental data. [21]

Figure 4 summarizes the variation of the Au-S and S-C bond lengths and the Au-S-C bond angle in the two stretching modes. We can note that both Au-S and S-C bond lengths increase during the stretching process of the molecular junctions. In the most stable structure, the Au-S bond length is 2.32 Å, and the Au-S-C bond angle 106.2°, in good agreement with reported values of 2.32 Å and 104.0°.[49] The Au-S-C bond angle is a little smaller than 109.5°, which is reasonable because of the strong steric repulsion between two lone-paired electrons on the sulfur atom. Such a trend changes the contact structures of the molecule and gold leads, and is further expected to affect the electrical properties of the molecular junction. We can note that bond lengths and angles of left and right contact geometries have the same cases that they are symmetrical changes in the double-end stretching. It is different for the single-end stretching mode that there are asymmetrical changes near the fracture point. The reason is mentioned above due to tensor shared more uniformly for double-end stretching system. It is worth noting that the Au atom at the top-pyramidal site of the electrode is at first pulled slightly out from the surface during the stretching process, followed then by the fracture of Au-S bond when the two electrodes are far enough away from each other. Finally, the tension in the system vanishes completely and the S-C bond length shortens rapidly at the fracture point. And the detailed structure evolution is shown in SI. These results show that the intramolecular geometric structures of the C-S and Au-S bonds, and the C-S-Au bond angle are very sensitive to the dynamic stretching process.

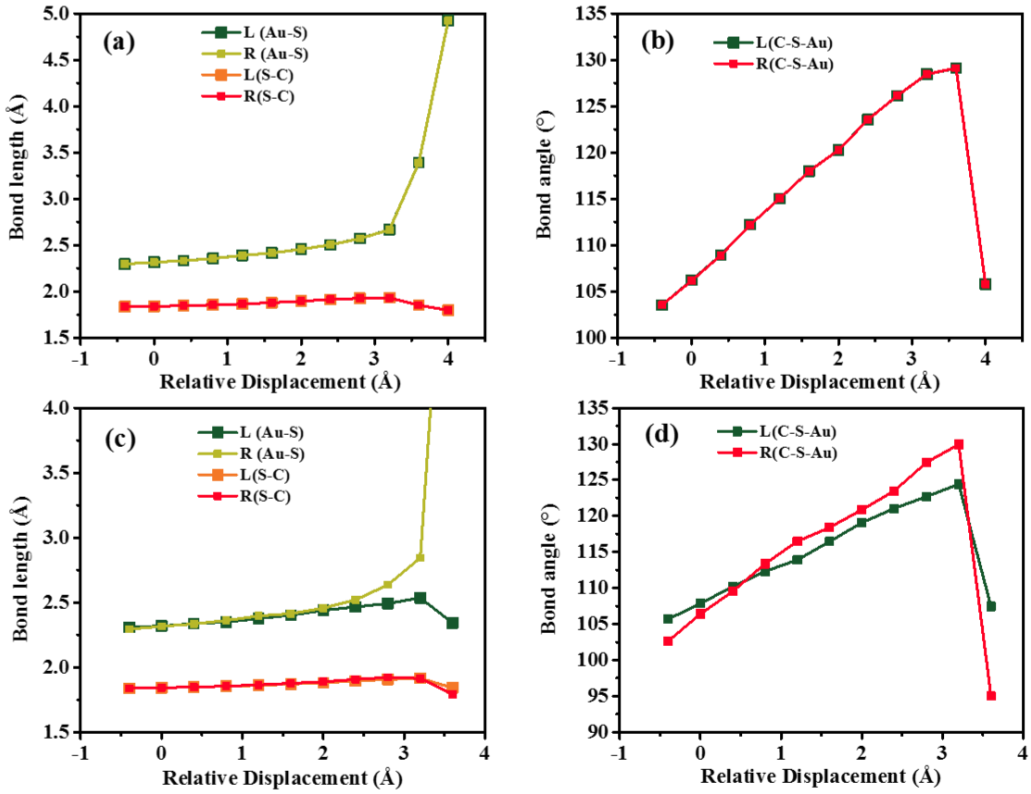

Figure 4. Variation of Au-S and S-C bond lengths and Au-S-C bond angles in the stretching processes of the gold-BDMT-gold junctions by two stretching modes. (a) Au-S and S-C bonds on the left and right sides in double-end stretching mode; (b) Au-S-C bond angle in the left and right sides of double-end stretching mode; (c) Au-S and S-C bonds in the left and right sides of single-end stretching mode; and (d) Au-S-C bond angle on the left and right sides in single-end stretching mode.

Distance-dependent Molecular Conductance. We pay attention then to the change of molecular quantum conductance during the stretching process. The molecular junction for double-end stretching here is firstly discussed, and as is mentioned above, the molecular junction of energy minimum with the length of 3.27 nm refers to the zero point. The current-voltage curves and zero-bias conductance at different lengths of the molecular junctions are shown in Figure 5. As shown in Figure 5a, the increase of the junction distance results in significant decrease of the slope of the current-voltage curves. This phenomenon is observed in previous experimental work[54] and further demonstrated in the variation of the molecular conductance in Figure 5b.

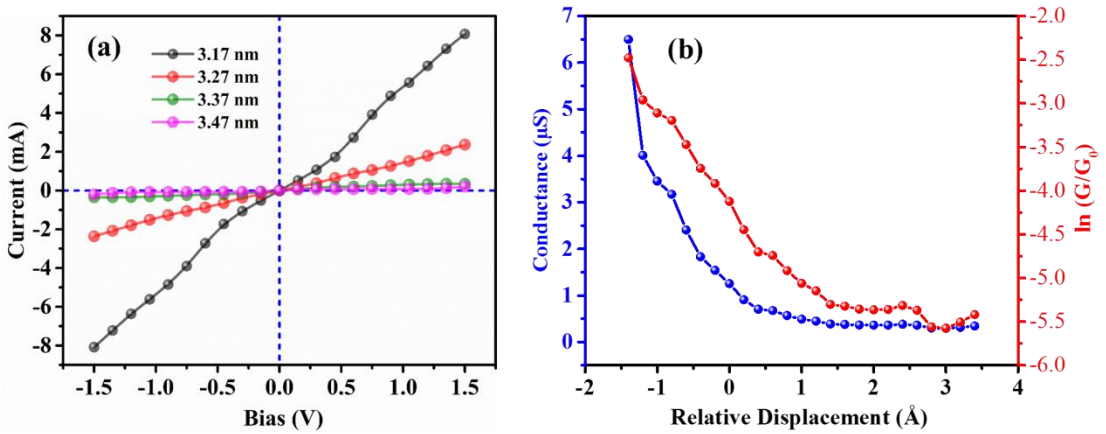

Figure 5. (a) Current-voltage curves and (b) conductance-distance relation of the gold-BDMT-gold double-end stretching junctions with different stretching lengths. In (b), the zero-bias conductance (blue line, left axis) together with a logarithmic correlation (red line, right axis) along the central region length are shown.

Figure 5b shows the variation of the zero-bias conductance with the stretching distance of the gold-BDMT-gold junction. The configuration of the molecular junctions strongly depends on the stretching distances (Figure S1). At the same time, the conductance decreases by about two orders of magnitude as stretching length increases. Conductance decreases exponentially indicating that electron tunneling from one electrode to the other is attenuated as the gap between the two gold leads widens. From Figure 5b, we can estimate the zero-bias conductance to be about 1.25 μS at the most stable structure of 3.27 nm, which is 15-fold larger than reported experimental values (46.5 nS).[31,47] However, when the nanogap size widens to about 3.4 nm, we obtain a conductance value decreasing to 294 nS, which is about 6-fold larger than the experimental value. As the molecular junction widens, the conductance at first decreases exponentially, and then flattens out. This indicates that the molecular conductance is observed at a dynamic stable structure. The quantum conductance profile is similar to the shape observed by STM.[24]

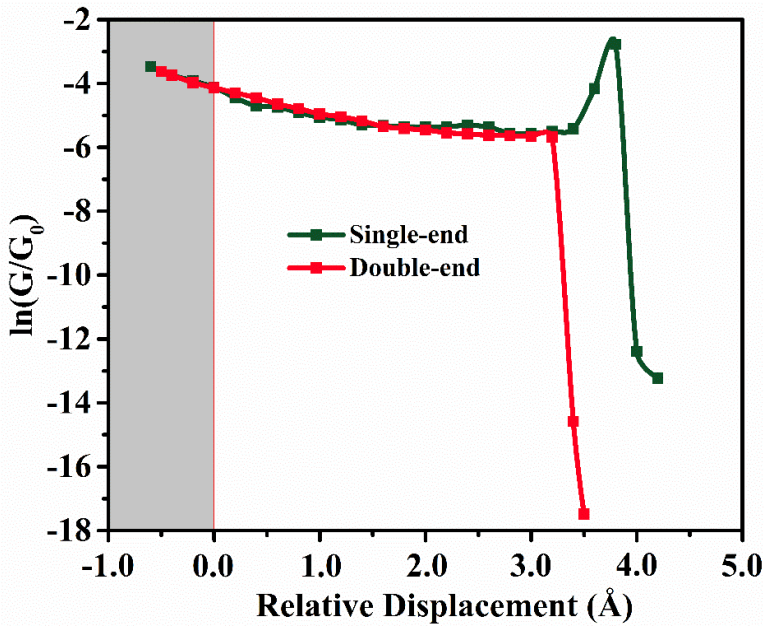

Figure 6. The conductance-distance logarithm relations of the gold-BDMT-gold junction with different stretching lengths in the top-pyramidal site. The red (solid sphere) and green (solid square) lines represent single-end and double-end stretching junctions, respectively.

Figure 6 presents the variation of the zero-bias conductance with increasing stretching distance of the gold-BDMT-gold junction in the two stretching modes. By comparing two modes, we can find both conductance at first decreases by about two orders of magnitude with increasing molecular junctions length. Then the conductance platform occurs in the single-end stretching junctions, while the conductance increase abnormally near the fracture point in the double-end stretching junctions. In order to understand the conductance decrease process, we have calculated the transmission spectra at different molecular junction lengths for two modes. We can find out molecular conductance mainly dominated by the highest occupied molecular orbital (HOMO) of the BDMT molecule at zero bias. With molecular junctions stretching, the HOMO energy level moves upwards to the Fermi level of gold electrodes, but the electronic coupling effect between the molecule and the electrodes decreases, and the width of the transmission peaks narrows, leading to the reduced conductance. However, there is an abnormal increase of conductance just before the fracture point in the double-end stretching mode, we shall explore this difference further in the next section.

Spin Splitting Effect on Molecular Conductance. In order to understand an abnormal increase in conductance in the double-end stretching mode before the fracture point well, we now pay our attention to the relation of Au-S bond length and molecular conductance, together with HOMO energy level of BDMT dominating electron tunneling, as shown in Figure 7a and 7b. Considering molecular junction elongation is mainly attributed to the Au-S bond length under stretching processes. Figure 7a shows that when the Au-S bond length is less than 2.44 Å, the conductance decrease exponentially. When the Au-S bond length is more than 2.44 Å, the conductance increase exponentially. This conductance phenomenon is same as shown in Figure 6 for the double-end stretching mode. Figure 7b shows that when the Au-S bond length is less than 2.44 Å, the HOMO level has not spin splitting, while when the Au-S bond length is larger than 2.44 Å, the HOMO level spin splitting occurs. In the case, we also find that the alpha electron spin moves downward away from the Fermi level of gold electrodes, in contrast to that the beta electron spin moves upward to the Fermi level. To obtain deep insight into the spin splitting effect on the molecular conductance, we further calculated spin dependent transmission spectra of α- and β- spin electrons (Figure 7c and 7d, respectively). The calculated results clearly show that the α-spin electron transport has little contribution to zero-bias conductance, while the contribution of β-spin transport gets more and more significant, finally resulting in greater resonance tunneling under stretching process. The β-spin electron contributes significantly to the increase of the molecular conductance (Figure 7d).

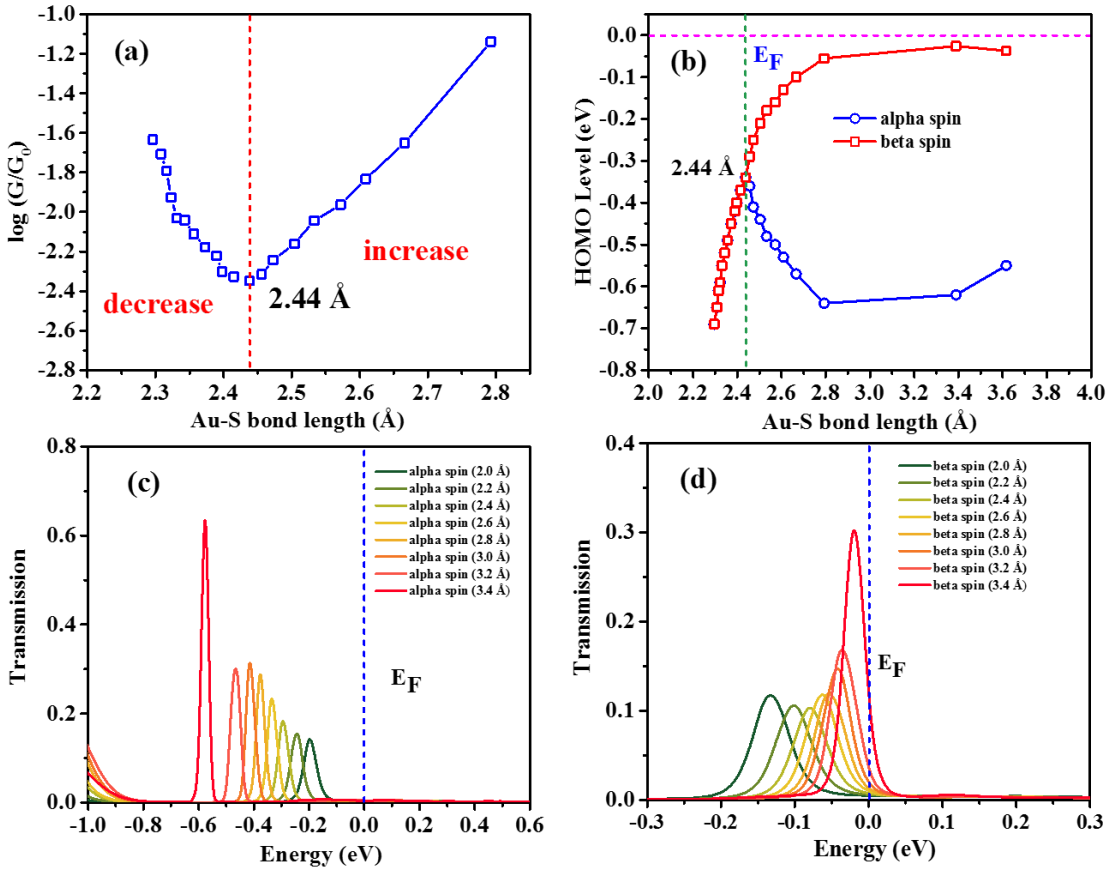

Figure 7. Distance-dependent variation of the molecular conductance (a) closely associated with (b) double-end, and both Au-S bonds at interfacial structures, (c) α-, and (d) β-spin electron transmission spectra in the top-pyramidal site of Au-BDMT-Au junctions at zero bias voltage.

As noted, when the molecular junction is further stretched, the conductance keeps a roughly constant value, and near the fracture points the conductance increases sharply in the double-end stretching mode, while no such phenomenon appears in the single-end stretching mode. This result also appeared in other theoretical [35,53] and experimental studies[55], but so far there are few clear rationales. In a previous study, this phenomenon was explained as caused by impure spin or doublet states of α- and β-spin electrons induced by the unpaired electron on the thiyl S· atoms during the fracture.[34,35] To understand the phenomenon further, the variation of the surface configurations can be appreciated by comparing the Au-S and C-S bond lengths of the two stretching modes (Figure 4). Similar changes appear on the left and right interfaces for the double-end stretching mode, while there are large differences between the two interfaces in the single-end stretching mode. The abnormal increase of the molecular

conductance is therefore closely related to the change of interfacial molecular structures in the stretching processes.

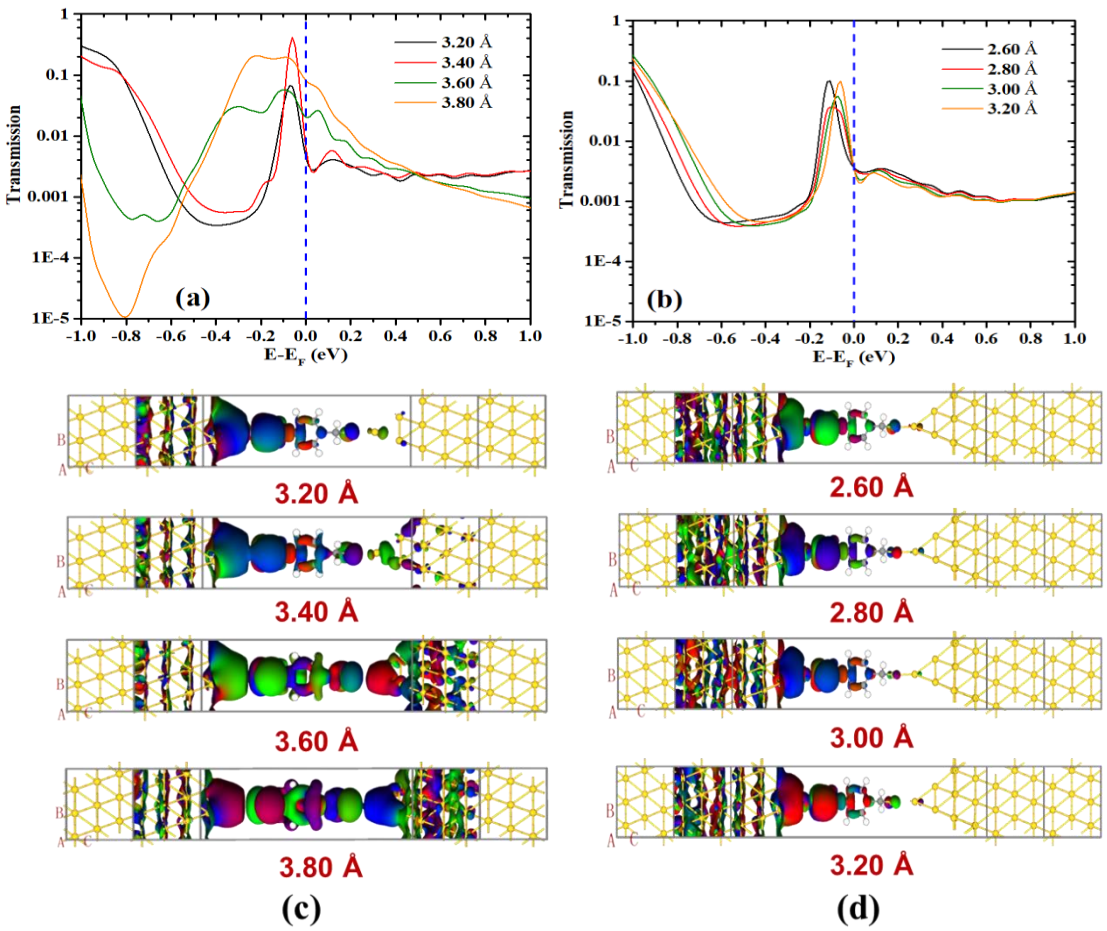

Figure 8. Comparison of transmission spectra with y-axis on logarithmic scale (upper row) and the spatial distribution MPSH HOMO orbitals (lower row) at the Fermi level for double-end (left, a and c) and single-end (right, b and d) stretching junctions just before the fracture point.

We further calculated the transmission spectra and MPSH of two stretching modes under pulling near the fracture point (Figure 8). The HOMO upshift towards the Fermi levels triggers the resonant tunneling in Figure 7b. This can be proved from the transmission spectra on logarithmic scale, where the larger junction distance results in the significant increase of the molecular conductance at zero bias in double-end stretching mode, shown in Figure 8a, whereas the conductance remains roughly constant for the single-end stretching mode, shown in Figure 8b. This can be understood from the difference of MPSH. It is also seen that the density of states is more delocalized for double-end stretching (Figure 8c), but only locally distributed at the left

end of the molecular junction and almost unchanged for single-end stretching (Figure 8d). These suggest why the molecular conductance changes differently near the fracture point for the two stretching modes.

Adsorption Site Effects. We would like to emphasize finally the effects of different adsorption sites on the relative stability energy,[56,57] stretching forces, and molecular conductance. The molecular junctions investigated here are the single-end stretching modes. Figure 9 shows the total electronic energies, the molecular conductance, and the stretching forces of optimized Au-BDMT-Au molecular junctions at the three different adsorption configurations, top-pyramidal, top, and bridge sites. The fracture point and energy curves are clearly different for different adsorption configurations. For example, there are more than a zigzag shape at which the energy curve significantly decreases at the bridge site, reflecting important relaxation features of the adsorption structure during the dynamic stretching process.

For molecular junctions of top-pyramidal and top sites, the Au atom binding to BDMT is firstly pulled out of the electrode surface. This pulling mode is reminiscent of the atomic scale "gold mining" in the adsorption of sterically unhindered alkanethiol molecules on Au(111)-electrode surfaces.[58,59] In previous studies, when organic dithiols are adsorbed at gold leads, the fracture of Au-Au bond was proposed experimentally and theoretically.[52,60,61] However, it is possible that the Au-S bond is also proposed to be broken at the fracture point as the distance between the electrodes increases.[34,35,62,63] For the molecular junctions with the sulfur atom binding at the hollow site, the stable configuration was optimized to transform from the hollow site to a bridge site after force convergence. As the right electrode is stretched, one of the Au atoms is pulled out of the gold surface followed by sequential fracture of the Au-S bond for the top-pyramidal site, while the fracture occurs at the Au-Au bond for the top site. Which is due to that the binding energy of the Au atom of the top-pyramidal site is larger than the top site. By inspection of the adsorption configurations along the energy curves, we noted turning points on the energy and stretching force curves, as shown in Figures S1-S3. This corresponds to the deformation of adsorption configurations from the bridge site to the top site during the stretching processes.

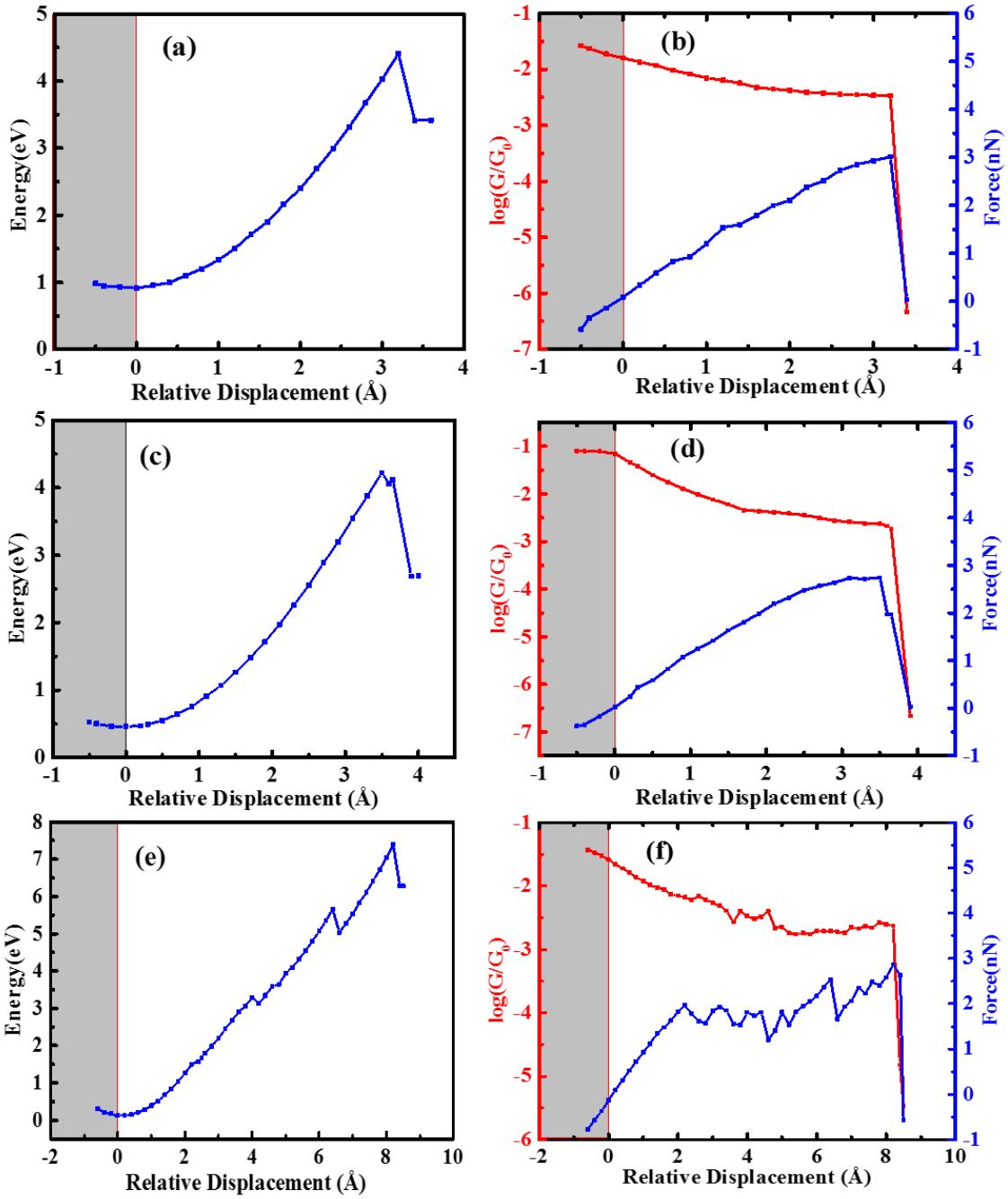

Figure 9. (a, c, and e) Relative electronic energies (black lines), (b, d, and f) zero-bias conductance (red lines) and stretching forces (blue lines) of the optimized Au-BDMT-Au molecular junctions at different adsorption sites (relative to the lowest energy in each series). (a and b) Top-pyramidal site; (c and d) Top site; and (e and f) Bridge site.

The variation of the stretching forces is slightly more complex than the potential energy curves and the molecular conductance (Figure 9f). The magnitude of the average force is about 2.0 nN. This was estimated from the derivatives of the potential energy

curves with respect to the distance change of the molecular junctions. The stretching forces are slightly the common value of 1.2 ~ 1.8 nN for the fracture of Au-Au bond from the force spectra of AFM measurements on 1,8-octanedithiol molecular junction[52] and dynamic theoretical values[21]. This closely accords with the local structure of molecular structures and different from experimental conditions.[21, 57]

We estimated the stretching force at different adsorption configurations. The maximum forces estimated at the fracture point of the top-pyramidal, top, and bridge adsorption sites are 19.34 eV/nm (3.10 nN), 18.03 eV/nm (2.89 nN), and 18.36 eV/nm (2.94 nN) corresponding to the Au-S bond and the Au-Au bond at fracture points, respectively. These stretching forces correspond to the sulfur atom binding to a gold atom at the top site on a gold surface. They are the steady state fracture force approaching to the fracture and are expected to be larger than that at the force loading rate, as suggested for the fracture of Au-Au bond .[21,57] In the bridge site junction, there is a significant fluctuation region at 2.0 ~ 4.0 Å with an average stretching force about 12.30 eV/nm (1.97 nN) in Figure 9f.[52] By inspecting the interfacial structures, we concluded that the forces arise from structural fluctuations with a reorganization of the surface gold atoms during the stretching process. The fluctuations of the stretching force can be observed at the molecular junction of the sulfur atoms adsorbed at the bridge sites (Figure 9f) and are closely associated with a significant variation in the relaxation of interfacial structures

We emphasize that the conductance generally drops prior to the fracture. We estimated the conductance values as 3.41×10^{-3} G_0 (264 nS), 1.78×10^{-3} G_0 (138 nS) and 1.73×10^{-3} G_0 (134 nS) at the top-pyramidal, top, and bridge sites, respectively. The latter two conductance values are about 3-fold larger than the experimental value (46.5 nS).[27,43] Our calculated results propose that the smaller conductance not only arises from the top site, but also that at a stretched junction under the external tensile loading. The experimental conductance of the molecular wire can be considered as that from the molecular configuration adsorbed at the top site. In this case the molecular junctions deviate from their minima and are stretched right up to the fracture.

In summary, the magnitude of molecular conductance measured in stretching

mode should correspond to the mechanical fracture point in the stretching process. The recorded molecular conductance and stretching forces reflect the dynamic evolution of interfacial structures and energy level alignments, including the different adsorption sites, chemical bond fission and electronic spin splitting. The theoretical results show that the steep molecular conductance increase is closely associated with the Au-S bond fracture and electron delocalization in the double-end mode. This is different from the fracture of Au-Au bond and the localized HOMO orbital in the single-end mode. The variation and steep increase of molecular conductance observed experimentally should therefore be an indicator for the fracture point at the Au-S bond when the molecular junction is stretched.

Conclusion

Using a combination of DFT and non-equilibrium Green's function calculations, we have explored a molecular junction, in which BDMT is trapped between two model Au-electrodes mimicking STM, mechanically controlled break junctions, or AFM. We considered BDMT in three different surface adsorption modes, i.e. top-pyramidal, top, and bridge sites in the gold nanogaps. Our focus was to follow the whole stretching process in the two enclosing electrodes, i.e. model substrate and model tip electrode are stretched from each other all the way from the equilibrium to a complete fission of the single- or double Au-S links. We could, particularly follow in minute detail all the bond length and bond angle changes in the bound BDMT, the molecular electronic conductivity changes, as well as the electronic frontier orbital (HOMO) changes and the alpha and beta electronic spin splitting that accompany the junction retraction, bond relaxation, and ultimate Au-S bond fission.

We first mapped the energy and force variation with electrode stretched, and found it to display smooth distance decreases up to the fracture point, followed by abrupt decrease of the conductance. The bond length and bond angles showed a parallel pattern with smooth and relatively small variation up to the fracture point followed by a strong Au-S bond length increase and bond angle decrease at the fracture point. Somewhat

unexpectedly, Au-S single- and double-bonded modes showed only relatively minor differences, with Au-S double-bonded BDMT having the longest stretching length, even though the bond fracture involves both Au-S bond fission and fracture between a surface Au-atom and the underlying substrate or tip.

The conductance/distance correlation is smooth (approximately exponential) up to the fracture point. This follows experimental STM observations, although the computed absolute conductance values are somewhat larger than the experimental values. This is likely to be associated with the underestimate of the HOMO-LUMO gap or overestimation of the Fermi level value by the PBE exchange correlation functional approach used. An improved functional approach would thus be desirable in further research. The double-end, but not the single-end stretching junction showed a puzzling local maximum in the conductivity-distance correlation at the fracture point (for example Figure 6). The conductance-distance correlations could be further illuminated in detail by the computed electronic transmission spectra and the splitting of the electron spin in the thiyl radical (HOMO) in the Au-S bonds into an alpha and a beta component. The computations showed a detailed and subtle interplay between the HOMO approaches to the Fermi levels of the enclosing electrodes and the alpha/beta splitting, as the Au-S bond lengths increase with increasing relative electrode distance. These effects also open new resonance tunneling channels as well as being reflected in characteristic distance dependent electronic density redistribution features for the double-end stretching mode in particular.

The DFT-NEGF approach presently used has thus offered novel and detailed insight into all the combined electronic structural, stretching force, and electronic conductivity properties of single- and double-end Au-S stretching BDMT in the gold enclosing molecular junction. Subtle effects such as the fine-structure in the conductivity-distance correlations, the electronic spin splitting, and the spin splitting effects in mechanistic controlling conductivity have been disclosed in the study. It can be expected that such comprehensive characterization can become a further useful and general guide to the stability and reactivity of thiyl-trapped molecular junctions and hopefully also to molecular targets trapped via other kinds of linker units.

Supporting Information

Optimized structures, the total energy, single-molecule conductance and force in the molecular junctions with sulfur atoms adsorbed at the top-pyramidal site, top site, and bridge site with the stretching processes.

Acknowledgements

We acknowledge support from the National Natural Science Foundation of China (NSFC) (Nos. 21773197, 22032004, 21533006, 21703183), the Chinese Ministry of Science and Technology (Y2018YFC1602802) and Funds of State Key Laboratory of Physical Chemistry of Solid surface and Fujian Science and Technology Office. DYW thanks Prof. Jingdong Zhang for her help to apply a visiting professorship from Otto Mønsted foundation in Denmark.

Key words

Adsorption site; Density functional theory; Para-benzenedimethanethiol; Single molecular junction fracture; Spin splitting effect

References

[1] J. E. Green, J. W. Choi, A. Boukai, Y. Bunimovich, E. Johnston-Halperin, E. Deionno, Y. Luo, B. A. Sheriff, K. Xu, Y. S. Shin, *Nature*, **2007**, *445*, 414-417.

[2] J. Martinez-Blanco, C. Nacci, S. C. Erwin, K. Kanisawa, E. Locane, M. Thomas, F. von Oppen, P. W. Brouwer, S. Foelsch, *Nat. Phys.* **2015**, *11*, 640-644.

[3] W. Y. Kim, K. S. Kim, *Nat. Nanotech*. **2008**, *3*, 408-412.

[4] S. Kaneko, Y. Hashikawa, S. Fujii, Y. Murata, M. Kiguchi, *ChemPhysChem* **2017**, *18*, 1229-1233.

[5] S. Kaneko, R. Takahashi, S. Fujii, T. Nishino, M. Kiguchi, *Phys. Chem. Chem. Phys.* **2017**, *19*, 9843-9848.

[6] (a) C. J. Lambert, Chem. Soc. Rev., **2015**, *44*, 875-888; (b) B. Xu, P. Zhang, X. Li, N. Tao, *Nano Lett*. **2004**, *4*, 1105-1108.

[7] D. Stewart, D. Ohlberg, P. Beck, Y. Chen, R. S. Williams, J. O. Jeppesen, K. Nielsen, J. F. Stoddart, *Nano Lett*. **2004**, *4*, 133-136.

[8] M. L. Chabinyc, X. Chen, R. E. Holmlin, H. Jacobs, H. Skulason, C. D. Frisbie, V. Mujica, M. A. Ratner, M. A. Rampi, G. M. Whitesides, *J. Am. Chem. Soc.* **2002**, *124*,

11730-11736.

[9] Y. Cai, A. Zhang, Y. P. Feng, C. Zhang, *J. Chem. Phys.* **2011**, *135*, 184703.

[10] F. Meng, Y. M. Hervault, Q. Shao, B. Hu, L. Norel, S. Rigaut, X. Chen, *Nat. Commun.* **2014**, *5*, 3023.

[11] (a) S. N. Yaliraki, M. Kemp, M. A. Ratner, *J. Am. Chem. Soc.,* **1999**, *121*, 3428-3434; (b) H. Basch, M. A. Ratner, *J. Chem. Phys*., **2003**, *119*, 11926-11942.

[12] S. Fujii, M. Koike, T. Nishino, Y. Shoji, T. Suzuki, T. Fukushima, M. Kiguchi, *J. Am. Chem. Soc.*, **2019**, *141*, 18544-18550.

[13] Y. Selzer, U. Peskin, *J. Phys. Chem. C*, **2013**, *117*, 22369-22376.

[14] J. H. Tian, B. Liu, X. L. Li, Z. L. Yang, B. Ren, S. T. Wu, N. J. Tao, Z. Q. Tian, *J. Am. Chem. Soc.*, **2006**, *128*, 14748–14749.

[15] X. S. Zhou, Y. M. Wei, L. Liu, Z. B. Chen, J. Tang, B. W. Mao, *J. Am. Chem. Soc.*, **2008**, *130*, 13228-13230.

[16] A. V. Walker, *J. Vac. Sci. Technol. A*, **2013**, *31*, 050816.

[17] J. H. Tian, Y. Yang, X. S. Zhou, B. Schöllhorn, E. Maisonhaute, Z. B. Chen, F. Z. Yang, Y. Chen, C. Amatore, B. W. Mao, *ChemPhysChem*, **2010**, *11*, 2745-2755.

[18] Y. Yoon, S. Noh, J. Jeong, K Park, *Ultramicroscopy*, **2018**, *188*, 70-76.

[19] W. E. Fu, K. Sivashanmugan, J. D. Liao, Y. Y. Lin, K. H. Cheng, B. H. Liu, J. J. Yan, M. H. Yeh, *Biointerphases*, **2016**, *11*, 04B311.

[20] B. Xu, N. J. Tao, *Science*, **2003**, *301*, 1221-1223.

[21] I. V. Pobelov, K. P. Lauritzen, K. Yoshida, A. Jensen, G. Meszaros, K. W. Jacobsen, M. Strange, T. Wandlowski, G. C. Solomon, *Nat. Commun.*, **2017**, *8*, 15931.

[22] G. C. Solomon, *J. Phys. Chem. C*, **2017**, *121*, 14381-14381.

[23] A. Pirrotta, L. De Vico, G. C. Solomon, I. Franco, *J. Phys. Chem. C*, **2017**, *146*, 092329.

[24] J. T. Zheng, R. W. Yan, J. H. Tian, J. Y. Liu, L. Q. Pei, D. Y. Wu, K. Dai, Y. Yang, S. Jin, W. J. Hong, Z. Q. Tian, *Electrochim. Acta*, **2016**, *200*, 268-275.

[25] L. O. Jones, M. A. Mosquera, G. C. Schatz, M. A. Ratner, *J. Phys. Chem. B*, 2019, 123, 8096-8102.

[26] A. Taninaka, S. Yoshida, Y. Sugita, O. Takeuchi, H. Shigekawa, *Nanoscale* **2019**,

11, 5951-5959.

[27] H. C. Wang, Y. S. Leng, *J. Phys. Chem. C*, **2015**, *119*, 15216-15223.

[28] D. Kruger, H. Fuchs, R. Rousseau, D. Marx, M. Parrinello, *Phys. Rev. Lett.*, **2002**, *89*, 186402.

[29] R. W. Yan, X. Jin, S. Y. Guan, X. G. Zhang, R. Pang, Z. Q. Tian, D. Y. Wu, B. W. Mao, *J. Phys. Chem. C*, **2016**, *120*, 11820-11830.

[30] V. Burtman, A. S. Ndobe, Z. V. Vardeny, *J. Appl. Phys.*, **2005**, *98*, 034314.

[31] X. Y. Xiao, B. Q. Xu, N. J. Tao, *Nano Lett.*, **2004**, *4*, 267-271.

[32] T. Dadosh, Y. Gordin1, R. Krahne, I. Khivrich, D. Mahalu, V. Frydman, J. Sperling, A. Yacoby, I. Bar-Joseph, *Nature*, **2005**, *436*, 677-680.

[33] C. Brooke, A. Vezzoli, S. J. Higgins, L. A. Zotti, J. J. Palacios, R. J. Nichols, *Phys. Rev. B*., **2015**, *91*, 195438.

[34] R. C. Hoft, M. J. Ford, M. B. Cortie, *Chem. Phys. Lett.*, **2006**, *429*, 503-506.

[35] R. C. Hoft, M. J. Ford, V. M. García-Suárez, C. J. Lambert, M. B. Cortie, *J. Phys. Condens. Matter*, **2008**, *20*, 025207.

[36] R. C. Hoft, M. J. Ford, M. B. Cortie, *Mol. Simul.*, **2007**, *33*, 897-904.

[37] Z. Y. Ning, J. Z. Chen, S. M. Hou, J. X. Zhang, Z. Y. Liang, J. Zhang, R. S. Han, *Phys. Rev. B*., **2005**, *72*, 155403.

[38] J. P. Perdew, K. Burke, M. Ernzerhof, *Phys. Rev. Lett*., **1996**, *77*, 3865.

[39] K. H. Müller, *Phys. Rev. B: Condens. Matter Mater. Phys.*, **2006**, *73*, 045403.

[40] H. Liu, Z. Zhao, N. Wang, C. Yu, J. Zhao, *J. Comput. Chem.*, **2011**, *32*, 1687-1693.

[41] K. Stokbro, D. E. Petersen, S. Smidstrup, A. Blom, M. Ipsen, K. Kaasbjerg, *Phys. Rev. B*, **2010**, *82*, 075420.

[42] Y. Xue, M. A. Ratner, *Phys. Rev. B*, **2003**, *68*, 115406.

[43] H. Grönbeck, M. Walter, H. Häkkinen, *J. Am. Chem. Soc*., **2006**, *128*, 10268-10275.

[44] Y. Li, X. C. Tu, M. L. Wang, H. Wang, S. Sanvito, S. M. Hou, *J. Chem. Phys.* **2014**, *141*, 174702.

[45] A. Changela, K. Chen, Y. Xue, J. Holschen, C. E. Outten,T. V. O'Halloran, A. Mondragón, *Science*, **2003**, *301*, 1383-1387.

[46] M. Büttiker, Y. Imry, R. Landauer, S. Pinhas, *Phys. Rev. B*, **1985**, *31*, 6207.

[47] C. Toher, S. Sanvito, *Phys. Rev. B*, **2008**, *77*, 155402.

[48] Y. Y. Liang, H. Chen, H. Mizuseki, Y. Kawazoe, *J. Chem. Phys.* **2011**, *134*, 144113.

[49] W. Y. Kim, K. S. Kim, *J. Comput. Chem.* **2008**, *29*, 1073-1083.

[50] Y. Cho, W. Y. Kim, K. S. Kim, *J. Phys. Chem. A* **2009**, *113*, 4100-4104.

[51] W. Hu, Q. L. Wang, Q. H. Zhou, W. H. Liu, Y. Liang, J. F. Hu, H. Q. Wan, *Can. J. Phys.*, 2020, *98*, 11-15.

[52] B. Q. Xu, X. Y. Xiao, N. J. Tao, *J. Am. Chem. Soc.*, **2003**, *125*, 16164-16165.

[53] L. Yuan D. Thompson L.; Cao N. Nerngchangnong C. A. Nijhuis, *J. Phys. Chem. C*, **2015**, *119*, 17910-17919.

[54] A. Borges, E. D. Fung, F. Ng, L. Venkataraman, G. C. Solomon, *J. Phys. Chem. Lett*, **2016**, *7*, 4825-4829.

[55] A. Torres, R. B. Pontes, A. J. R. da Silva, A. Fazzio, *Phys. Chem. Chem. Phys.* **2015**, *17*, 5386-5392.

[56] W. Lee, P. Reddy, *Nanotechnology*, **2011**, *22*, 485703.

[57] K. E. Drexler, K. E., Nanosystems - Molecular Machinery, Manufacturing, and Computation, John Wiley & Sons, New York, 1992.

[58] Y. Wang, Q. Chi, N. S. Hush, J. R. Reimers, J. Zhang, J. Ulstrup, *J. Phys. Chem. C* **2009**, *115*, 10630-10639.

[59] Y. Wang, Q. Chi, J. Zhang, N. S. Hush, J. R. Reimers, J. Ulstrup, *J. Am. Chem. Soc.,* **2011**. *133*, 14856-14859.

[60] C. Nef, P. L. T. M. Frederix, J. Brunner, C. Schönenberger, M. Calame, *Nanotechnology*, **2012**, *23*, 365201.

[61] M. Tsutsui, M. Taniguchi, T. Kawai, *Nano Letters*, **2009**, *9*, 2433-2439.

[62] C. Bruot, J. Hihath, N. J. Tao, *Nat. Nanotech.* **2012**, *7*, 35-40.

[63] Y. Jiang, Q. Huan, L. Fabris, G. C. Bazan, W. Ho, *Nat. Chem.*, **2013**, *5*, 36-41.

Table of Contents

The conductance and electron tunneling method of Au-BDMT-Au molecular junction are related to the length, adsorption sites, and stretching processes. As the molecular junction is stretched, the conductance decreases exponentially at first and then become flat before fracture. We also find an abnormal increase at the fracture point of the double-end stretching junction. That is explained due to the spin splitting effect resulting in the resonant tunneling of electrons in the double-end stretching junctions.